Shabanpour, Javad; Simovski, Constantin R.

Angular and polarization stability of broadband reconfigurable intelligent surfaces of binary type

Published in:
IEEE Access

DOI:
10.1109/ACCESS.2022.3226264

Published: 01/01/2022

Document Version
Publisher's PDF, also known as Version of record

IEEE Access
Multidisciplinary ⋮ Rapid Review ⋮ Open Access Journal

Received 3 November 2022, accepted 25 November 2022, date of publication 1 December 2022,
date of current version 7 December 2022.

Digital Object Identifier 10.1109/ACCESS.2022.3226264

RESEARCH ARTICLE

Angular and Polarization Stability of Broadband Reconfigurable Intelligent Surfaces of Binary Type

JAVAD SHABANPOUR, (Graduate Student Member, IEEE), AND CONSTANTIN R. SIMOVSKI

Department of Electronics and Nanoengineering, School of Electrical Engineering, Aalto University, 02150 Espoo, Finland

Corresponding author: Javad Shabanpour (mohammadjavad.shabanpoursheshpoli@aalto.fi)

This paper is accomplished within the framework of Meta Wireless project which has received Full Funding from the European Union's Horizon 2020 research and innovation programme under the Marie Sklodowska–Curie grant agreement No 956256.

ABSTRACT Recently, reconfigurable intelligent surfaces (RISs) gained notable consideration due to their ability to provide efficient and cost-effective wireless communication networks. However, this powerful concept often suffers from simplistic modeling which underestimates such features of RIS as the resonant frequency dispersion and strong angular dependency of the reflection phases for both TE and TM polarizations of the incident wave. The angular and polarization instability of the reflection phase is a fundamental restriction of RISs, especially restrictive if the operation frequency band is broad. In this paper, we address this challenge for a binary RIS performed as a metasurface. We have studied the reflection phase frequency dispersion (RPFD) analytically that allowed us to engineer the needed angular and polarization properties of the RIS. Our RIS is a self-resonant grid of Jerusalem crosses located on a thin metal-backed dielectric substrate. Adjacent crosses are connected by switchable capacitive loads. We have shown the advantage of our metasurface compared to switchable mushroom-field structures and meta-gratings of resonant patches. An RIS is also fabricated and measured, and the experimental results corroborate well our numerical full wave simulations and analytical predictions.

INDEX TERMS Reconfigurable intelligent surface (RIS), wireless communication, angular stability.

I. INTRODUCTION

Evolution of telecommunications shifts wireless networks to higher frequencies. This shift can be attributed to a number of factors, including more reliable and safer communications, growing capacity requirements, more accurate localization of objects, and the demand for low-latency communication [1], [2], [3]. Novel frequency ranges – the millimeter-wave (mmWave) and terahertz (THz) ranges – allow much larger bandwidth, and much higher peak data rates for the fifth-generation (5G) and sixth generation (6G) cellular networks [4], [5]. Despite the benefits of mmWave communication, it still suffers from fundamental drawbacks, including large path loss which requires high power transmitters, high atmospheric absorption, parasitic multi-path interference, and shadowing by obstacles [6], [7]. Consequently, reaching smart, robust, and, above all, dynamic Line of Sight (LOS) communication, necessitate migrating toward the software-defined model for future, more reliable wireless communications.

In this framework, reconfigurable intelligent surfaces (RISs) have appeared as an optimistic enabling technology to empower future wireless networks [8], [9]. A RIS is a compact and low-power alternative to the relay base stations. RIS is analogous to a conventional reflect-array used in high-frequency antenna techniques so that to shape the radiated beam. It is an array of small, low-cost, and passive (though tunable) reflecting elements [10]. Compared to relays deployments and cell-free massive MIMO which increase the network power consumption, RISs grant such

The associate editor coordinating the review of this manuscript and approving it for publication was Li Zhang.

fundamental benefits as consuming small power (spent only for tuning the reflection phase of the elements), lower hardware complexity, lower cost, no self-interference, and no backhaul requirements [11]. Meanwhile, adaptive shaping of the wireless channels has made the RIS a promising candidate for smart radio environments [12], [13]. Recently, RISs have been used to realize the binary frequency shift-keying (BFSK) transmitter [14], multi-modulation schemes [15], IRS- assisted full-duplex wireless communications [16], MIMO-assisted networks [17], and non-orthogonal multiple access (NOMA) communication network [18].

Often, the RIS paradigm is considered within the programmable metasurface concept [6]. Metasurfaces (MSs) are defined as thin layer periodic arrangements of unit cells formed by thin sub-wavelength resonators [19], [20], [21]. Since the unit cell is much smaller than the wavelength, the metasurface (though resonant) can be treated as an effectively continuous surface enabling the smooth coordinate dependence of the reflection phase. The gradient of the reflection phase with respect to the tangential coordinate allows one to deflect the incident wave i.e. to manipulate the direction of the reflected wave. To deflect the incident beam with the angle θ to the deflection angle θ_r, one needs to use the MS whose reflection phase linearly varies from 0 to 2π within the period D. This period is determined by the two angles as [22]:

$$D = \frac{\lambda}{|\sin\theta - \sin\theta_r|}. \tag{1}$$

Here the angle θ_r is considered negative when the reflected wave vector is tilted to the same side as the incident wave vector with respect to the normal (i.e. the retro-reflection case corresponds to $\theta_r = -\theta$) [23], [24].

Of course, the continuous linear coordinate dependence of the reflection phase $\Phi_R(x) = 2\pi x/D$ is the ideal case. In reality, one may engineer unit cells of size Δx offering the discrete change of the reflection phase $\Delta\Phi_R = 2\pi\Delta x/D$ from cell to cell within one period. In conceptual papers such as [23] and [24], this gradual reflection phase variation was done via variation of the resonating element size from cell to cell within the period (non-tunable). For RIS, the same result was achieved using electronically controlled lumped loads (tunable) whereas the scattering elements in each unit cell were the same [25], [26], [27], [28], [29], [30].

This approach identifies a RIS to the MS with multiple discrete digital states and allows one to engineer the needed scattering pattern [29]. When the incidence angle changes or the reflection angle needs to be changed, one can change the biasing mechanism of the unit cells so that to properly change the phase shift $\Delta\Phi_R$ between two adjacent unit cells, and the period D changes accordingly. These tunable loads should be reactive to avoid the strong absorption of the incident signal (which needs to be reflected and not absorbed).

The drawback of this technical solution is its high cost. To achieve multiple values of the reactive loads in each element of the MS reliably and without parasitic losses, an expensive electronic circuitry is needed, especially if the operating frequencies are high and parasitic losses in the loads are noticeable. The simplest and cheapest version of the RIS that is performed as an MS is the binary MS: two values of the load e.g. capacitances C_1 and C_2 that grant two reflection phases – those with the phase difference $\Delta\Phi_R = \pi$. This approach allows the unit cell to mimic two digital states – '0' and '1'. Being easier to implement and cheaper to fabricate and exploit, especially at the biasing point, binary MSs have got a hot topic status in the modern literature on RISs [2], [16], [25].

It can be thought that the replacement of a metasurface with multiple states (multi-bit) of a unit cell by a metasurface with only two states (binary) should result in a drastic worsening of its diffraction pattern. Let the unit cell size a equal $\lambda/10$ and $\theta_r = 30°$. Then the period D equals 2λ and there are 20 unit cells in the period. In the multiple-state approach, we may use 20 different values of the loading capacitance. Thus, we seemingly mimic the linear reflection phase coordinate dependence $\Phi_R = 2\pi x/D$ by the step-wise function with the step as small as $360°/20 = 18°$ and as narrow as $\lambda/10$. Meanwhile, in the binary MS, the reflection phase varies with the step as large as π and as wide as $D/2 = \lambda$. In the period, 10 unit cells are in the state of '0', and 10 unit cells are in the state of '1'. This seems to be a much worse model of the reflection phase linear coordinate dependence. However, it is not so! The controllable deflection of the incident beam for the binary MS is not much worse than that granted by the 20-states unit cells. That fine-tuning of the unit cells implies, in fact, not the local reflection phase but the local surface impedance. The reflection of the incident wave by an array of unit cells is a collective process. It is determined not by the surface impedance of the given unit cell but by the distribution of the surface impedance in the effective spot of radius $\lambda/2$ around it. This is why periodical MSs formed by large groups of '0'-state unit cells alternating with the similar groups of '1'-state unit cells grant nearly the same quality of the diffraction angle as that granted by finely tuned periodical MSs (see e.g. in [30], [36], [37]). Albeit, it is obvious that due to the symmetry, the other deflected waves will be created at $\theta = -\theta_r$. By changing the number of the same unit cells in each group, the deflection angle can be tuned based on the generalized reflection law.

The tendency to further simplify the RISs resulted in the appearance of so-called periodical meta-gratings (MGs) [22]. Elements of a meta-grating have the tangential sizes of the order of $\lambda/2$. One element of the MG replaces a group of several unit cells of the MS performing the presumably same functionality [22], [31]. It was shown that MGs comprising three resonators per period D may grant the needed deflection with the same quality of the diffraction pattern as that of a metasurface with a number of subwavelength unit cells per the same period [32], [33], [34]. The MG can be binary as well. Then the resonators of the MG are all identical and the difference between their responses is ensured by the switchable load [35].

Though the progress of RIS in the literature is indisputable, there are still dark points in this field. The majority of papers about RIS-assisted communications use simplistic informational and theoretical tools. Often they model the RISs by ideal phase shifters neglecting the inherent electromagnetic behavior of the MSs, their dispersion, their angular instability, the non-locality of their reflection coefficient etc. [36], [38], [39], [40]. These optimistic models can not expose the RISs behavior in real wireless communication systems. Conceptual papers that correctly treat RISs from the electromagnetic point of view, consider them operating at a single frequency. Meanwhile, 5G telecommunication systems and especially prospective 6G systems demand broadband operation. In practice, the relative frequency band is needed with relative width as large as 20% (i.e. $\pm 10\%$ around the central frequency). Is $\Delta\Phi_R$ close to π in such broadband frequency? These reflecting surfaces are resonant and their refection phase strongly varies versus frequency. Does it vary similarly in both states '0' and '1'? This issue was not studied in the available papers on binary MSs and MGs.

Another point is the angular stability of the reflection phase. It is a fundamental factor to keep the reconfigurable and real-time channel estimation [41], [42]. The frequency dispersion of the reflection phase may drastically change when the incidence angle changes. Moreover, for the given incidence angle θ, this change may be different for the TE-incident wave and for the TM-incident one. If so, the operation of the RIS (even broadband) for one direction of the incident beam will be destroyed when another beam will impinge on it from another polarization.

Formerly, some papers have brought forward the angular stability of resonance using high impedance surfaces (HIS). However, only partial stabilization has been obtained since most of them are dedicated to angular stability of just the single resonance frequency or for one polarization, see e.g. in [43], [44], [45], [46], [47], [48], and [49]. For a properly operating RIS, we need not simply the stable resonance versus the incidence angle. Our goal is to keep the states '0' and '1' within the wide band of the incidence angles and broadband of frequencies. Moreover, we need to achieve this robustness for both TE- and TM-polarizations of the incident wave. This is the problem we theoretically solve in the present paper. Our study reveals that the angular stability of the RPFD besides the stability of resonance frequency also demands the stability of the slopes. As a proof of concept, several illustrative examples are corroborated through numerical simulations and analytical models. Finally, by performing sets of experimental measurements, the angular and polarization stability of our proposed RIS in a broad range of frequency bands are well verified. The authors believe that the presented study is anticipated to expand the applications of switchable digital metasurfaces and especially appealing for the practical implementation of RISs. Since our study solves the RIS's angular sensitivity, a drawback that is neglected in the literature up to now, it can pave the way for practical real implementation of RIS-based wireless communication.

II. PROBLEM FORMULATION

A. BROADBAND OPERATION OF A BINARY METASURFACE

First, let us show that the operational band should either comprise the resonance frequencies ω_{01} and ω_{02} corresponding to both states '0' and '1' or be located in between these resonances.

The thickness of the MS in the whole range of our interest frequency is small, i.e. the substrate between the top grid and the ground plane is optically thin. Since it is metal-backed, it means that its surface impedance Z_- is inductive [50], does not matter is it a simple dielectric layer or a composite one. Let the needed MS be implemented as a periodic planar grid of metal elements located on the top of such the inductive substrate. Then its surface impedance is calculated as follows [50]:

$$Z_s = \frac{Z_g Z_-}{Z_g + Z_-} = \frac{(r_g r_- - X_g X_-) + j(r_g X_- + r_- X_g)}{r_\Sigma + jX_\Sigma}, \quad (2)$$

where Z_g is the sheet impedance of the grid taking into account the presence of the substrate, Z_- is the surface impedance of the metal-backed substrate, X_g and X_- are imaginary parts of Z_g and Z_-, r_g and r_- are real parts of Z_g and Z_- determined by losses (since our MS is not absorbing, we adopt that $r_g \ll X_g$, $r_- \ll X_-$). Also, in (2) we have denoted $r_\Sigma = r_g + r_-$, $X_\Sigma = X_g + X_-$.

In accordance to (2), the surface impedance Z_s is that of the termination of the transmission line emulating free space and represents a parallel connection of the inductive impedance Z_- and Z_g. If Z_g is also inductive, there is no resonance and we cannot noticeably change the reflection phase with the loading inductance. The only way to achieve a drastic change of the reflection phase via loading is to assume that X_g in (2) is capacitive, and in the operational band it should intersect with the resonance band in which Z_g resonates with Z_-. Beyond the resonance band, Z_s is low and operates nearly as a shortcut of the transmission line mimicking free space. Therefore, at low and high frequencies, its reflection phase is close to π independently of the load value. At the resonance, the MS behaves like a perfect magnetic wall (PMW), i.e. $\Phi_R = 0$ in the state '0' at frequency ω_{01} and $\Phi_R = 0$ in the state '1' at frequency ω_{02}. Since the cases $\Phi_R = \pi$ and $\Phi_R = -\pi$ are not distinguishable, it is reasonable to plot the reflection phase-frequency dispersion (RPFD) so that Φ_R varies from π at low frequencies to $-\pi$ at high frequencies. In the resonance band, function $\Phi_R(\omega)$ is approximately linear.

Now let us think about how to achieve nearly 180° phase difference between two states of the reflection phase-frequency dispersion if the frequency band of operation $[\omega_-, \omega_+]$ is broad. In Fig. 1, we qualitatively show all possible cases for the figure formed by two states of RPFD. In the real application, each of these two RPFDs should correspond to the local reflection coefficient of a group of unit cells in the same state. We should have in mind that the size of this group is $D/2$ which is of the order of λ. However, in the present work, we assume that this is the reflection phase of an infinite uniform MS. Therefore, the group of identical

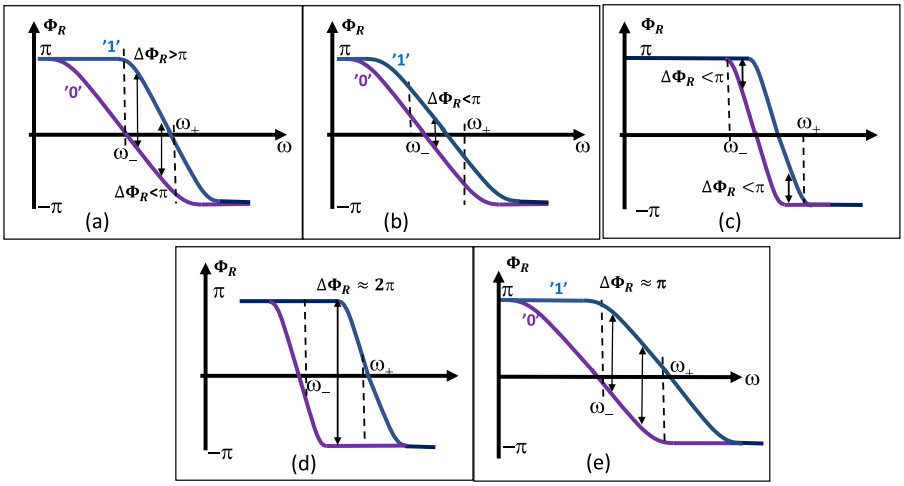

FIGURE 1. a) Unsuitable figure of the two-states RPFD. The slopes of two RPFDs are noticeably different. (b) Unsuitable figure of the two-states RPFD. The slope of the RPFDs is small, but the resonance frequencies ω_{01} and ω_{02} are not sufficiently different. (c) Unsuitable figure of the two-states RPFD. The slope of the RPFDs is large and the resonance frequencies ω_{01} and ω_{02} are not sufficiently different. (d) Unsuitable figure of the two-states RPFD. The resonance frequencies ω_{01} and ω_{02} are properly chosen, but the slope of two RPFDs is too large. e) The willow-leaf figure of two-states RPFD. The slope of the RPFDs is small and the resonant frequencies are properly chosen. In all figures (a-e) dashed vertical lines show the edges of the operation band ω_- and ω_+.

unit cells should be large enough, which implies a strongly subwavelength period a. We will design the MS to respect this condition, but the model of the local reflection coefficient of a periodic binary MS will be verified in our next work. The aim of the present work is to synthesize the infinite MS whose two-states RPFD ensures the broadband operation, weakly sensitive to the incidence angle and wave polarization.

Now let us see which type of the two-states RPFD grants the broadband operation. The first condition is an approximate equivalence of the slopes of two RPFDs corresponding to states '0' and '1'. In Fig. 1(a) we show the situation when these slopes are noticeably different. In this case, the broadband operation is not achievable. Even if we engineer $\Delta\Phi_R = \pi$ at the central frequency of the operation band, it will be larger than we need in one half of the band and smaller in another half. The second condition is the sufficient difference between the resonant frequencies. In the opposite case, i.e. when $(\omega_{02} - \omega_{01}) \ll (\omega_+ - \omega_-)$, we also cannot achieve the broadband operation. In fact, if the slope of RPFD is small, we come to the situation illustrated by Fig. 1(b), when $\Delta\Phi_R \ll \pi$ in the whole operation band. If the slope of the RPFD is large, we have the figure shown in Fig. 1(c), when $\Delta\Phi_R$ is also much smaller than π. The resonance frequencies are engineered properly when ω_{01} is rather close to ω_-, and ω_{02} is rather close to ω_+. However, this is not the guarantee of the broadband operation. In Fig. 1(d), we show the case when the slope of the RPFD is high. Then, in the most part of the operation band $\Delta\Phi_R \approx 2\pi$. Only in Fig. 1(e), the correct RPFD corresponds to the broadband operation of a binary MS is shown. We have called it "willow-leaf" two-states RPFD.

Our target is to design a RIS that keeps the same willow-leaf two-states RPFD when the incident angle θ varies within the maximally large band of angles $0 \le \theta \le \theta_{max}$ for both TE and TM polarizations.

B. ANGULAR AND POLARIZATION STABILITY OF THE WILLOW-LEAF DISPERSION FIGURE

For certainty, we specify the relative width of the operation band as 20% i.e. $(\omega_+ - \omega_-)/(\omega_+ + \omega_-) = 0.1$, and put the maximal allowed deviation of the reflection phase difference $\Delta\Phi_R$ from the target value 180° equal to 40°.

Ensuring the sufficient separation of the resonance frequencies ω_{01} and ω_{02} is easy. It is granted by the proper choice of the lumped loads. To achieve the angular stability of these frequencies, we have to analyze the angular dependence of the grid impedance and the substrate impedance for both TE and TM polarizations. In a qualitative approximation, the resonance corresponds to the equation $X_g(\omega, \theta) + X_-(\omega, \theta) = 0$. The solution of this equation does not depend on θ in two cases. First, when the angular dependence of X_g and X_- is the same (that is hardly possible for both polarizations). Second, when the θ- dependent terms cancel out in the resonance equation. Assume, that this is possible to implement for both polarizations.

After we have achieved the angular stability of the resonance frequencies for TE and TM cases, the next task is to achieve the low slope of the RPFDs, the same for two states and weakly varying versus θ. To understand how to obtain it, let us express the reflection coefficient R of a MS in the given state ('0' or '1') via the surface impedance Z_s and incident angle θ for TE and TM polarization cases. In accordance to [50] we have:

$$R^{TE} = \frac{Z_s^{TE}\cos\theta - \eta}{Z_s^{TE}\cos\theta + \eta}, \quad R^{TM} = \frac{Z_s^{TM} - \eta\cos\theta}{Z_s^{TM} + \eta\cos\theta}, \qquad (3)$$

where $\eta = \sqrt{\mu_0/\varepsilon_0}$ is the free-space wave impedance. The reflection coefficient of a MS is obviously depending on θ. This is so because in accordance to (2), Z_s is the parallel connection of Z_g and Z_-. For the metal-backed substrate (with or without vias), the angular dependence of Z_- does not allow to achieve $Z_s^{TE} \sim \cos^{-1}\theta$ simultaneously with $Z_s^{TM} \sim \cos\theta$ without making the resonance frequency ω_0 (at which $Z_s = \infty$ in the lossless approximation) dependent on θ. Meanwhile, the angular stability of the resonance for the given state of the MS is the most important condition of the willow-leaf figure's robustness. This observation means that the ideal angular stability of the reflection coefficient is not achievable. Since the absolute value of $r^{TE,TM}$ is nearly equal unity, it means that the angular stability of the reflection phase can be only approximate.

The reflection phase in the TM and TE cases can be expressed, respectively, by:

$$\Phi_R^{TM} = \arctan\left(\frac{X_s^{TM}}{r_s^{TM} - \eta\cos\theta}\right) - \arctan\left(\frac{X_s^{TM}}{r_s^{TM} + \eta\cos\theta}\right) \tag{4}$$

$$\Phi_R^{TE} = \arctan\left(\frac{X_s^{TE}\cos\theta}{r_s^{TE}\cos\theta - \eta}\right) - \arctan\left(\frac{X_s^{TE}\cos\theta}{r_s^{TE}\cos\theta + \eta}\right) \tag{5}$$

Here, in accordance to notations introduced above, $X_s^{TE,TM}$ and $r_s^{TE,TM}$ are imaginary and real parts of $Z_s^{TE,TM}$, respectively. At the resonance frequency, we have $X_s^{TE,TM} = 0$ i.e. the reflection phase nullifies.

The slope of the RPFD for any incidence angle is basically determined by the frequency derivative of Φ_R at the resonance frequency. For the TM case we have:

$$\Phi_R'(\omega_0,\theta) = \frac{X_s'(\omega_0,\theta)}{[r_s(\omega_0,\theta) - \eta\cos\theta]} - \frac{X_s{}'(\omega_0,\theta)}{[r_s(\omega_0,\theta) + \eta\cos\theta]}. \tag{6}$$

Deriving (6), we used the standard formula $\arctan'[y(x)] = y'(x)/[1 + y^2(x)]$ and the fact that $X_s(\omega_0) = 0$. Since at the resonance frequency the surface resistance attains its maximum and $r_s(\omega_0) \gg \eta$ the slope of RPFD in accordance to (6) takes form:

$$\Phi_R'(\omega_0,\theta) \approx \frac{2X_s'(\omega_0,\theta)\eta\cos\theta}{r_s^2(\omega_0,\theta)}. \tag{7}$$

The slope independency on θ can be granted e.g. by condition $r_s^2(\omega_0,\theta) \sim \cos\theta$ and $X_s'(\omega_0,\theta) = const(\theta)$.

Meanwhile, for the TE-case we have

$$\Phi_R'(\omega_0,\theta) = \frac{X_s'(\omega_0,\theta)\cos\theta}{[r_s(\omega_0,\theta)\cos\theta - \eta]} - \frac{X_s'(\omega_0,\theta)\cos\theta}{[r_s(\omega_0,\theta)\cos\theta + \eta]}. \tag{8}$$

Even though $r_s(\omega_0) \gg \eta$, for large incidence angles $\cos\theta \ll 1$ and the value $\eta/\cos\theta$ obviously becomes of the order of $r_s(\omega_0,\theta)$. Near $\theta = \pi/2$, there is obviously the angle for which $r_s(\omega_0,\theta)\cos\theta = \eta$. At this angle, the RPFD has a singular frequency derivative. The jump of the reflection phase versus frequency is the implication of the resonance because in the non-resonant case $r_s < \eta$ at any frequency and for any incidence angle. For a resonant metasurface, the angular stability of the RPFD slope for $\theta \approx \pi/2$ illuminated by TE-polarized or non-polarized waves is not achievable. Therefore we should restrict our consideration by modest angles, e.g. assuming $\theta_{max} = \pi/4$, we will have $r_s(\omega_0)\cos\theta \gg \eta$. Then the slope of the RPFD as follows from (8) equals to

$$\Phi_R'(\omega_0,\theta) \approx \frac{2X_s'(\omega_0,\theta)\eta}{r_s^2(\omega_0,\theta)}. \tag{9}$$

If $r_s(\omega_0)$ does not depend on θ the slope of RPFD is angle-independent for modest angles and TE-polarization.

It is difficult to simultaneously ensure $r_s^2(\omega_0,\theta) \sim \cos\theta$ for the angle-independent slope in the TM case and $r_s^2(\omega_0,\theta) = const(\theta)$ for the TE case. However, we formulated the criterion for $\Delta\Phi_R$ so that the relative deviations $\pm 20\%$ are allowed. The same refers to the deviations of the RPFD slope. When $\theta \leq \pi/4$ cosine function is weakly varying and the problem can be simplified. In accordance to (7) and (9) we have to engineer both $X'(\omega_0)$ and $r_s(\omega)$ independent on θ for both polarizations. This is a feasible task and below we manage it.

The next task is to make this reflection phase slope nearly the same and modest for the two states RPFD. It means that we have to make the slope of the unloaded and loaded $X_s(\omega)$ at two frequencies ω_{01} and ω_{02} nearly the same and modest. Consider the state '0'. In the approximation of the simple LC-resonance that is adequate for qualitative estimations, we have for the surface reactance in the state '0' $X_s^{(0)}(\omega) \approx \omega L - 1/\omega C_1$. Meanwhile, for the surface reactance in the state '1' we have $X_s^{(1)}(\omega) \approx \omega L - 1/\omega C_2$. In both cases, the frequency derivative of the reactance is equal to

$$X_s'(\omega_{01,02}) = L + \frac{1}{\omega_{01,02}^2 C_{1,2}} = 2L,$$

since $\omega_{01,02}^{-2} = LC_{1,2}$. So, the same slope of the reflection phase in two states is automatically secured if we make the switchable load capacitive. Next, the slope of the RPFD is angle-independent if the effective inductance of the MS does not depend on the incidence angle. We will see that it is possible for $\theta < \theta_{max}$ and incident wave polarizations if the sensible value for θ_{max} is specified. Finally, this slope is obviously low if the resonance band of the MS is broad. This is clear from the qualitative plots in Fig. 1.

So, our task is feasible – it is possible to engineer the willow-leaf dispersion figure which would be robust in a reasonably wide band of incidence angles for non-polarized waves.

III. INVESTIGATION, RESULTS AND DISCUSSION

A. THE BRIEF SUMMARY

Fig. 2(a) illustrates our main achievement. Our MS comprises the grid of Jerusalem crosses connected by pin-diodes. The grid is located on top of a thin metal-backed dielectric layer

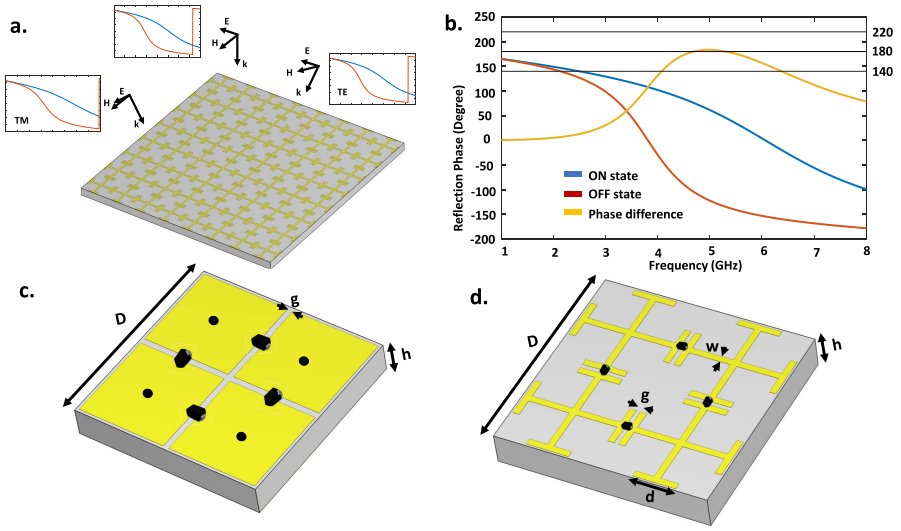

FIGURE 2. a) Sketch representation of the proposed binary RIS. The insets depict the willow-leaf dispersion figure for θ_{max} when the structure is illuminated by the TE and TM polarized waves incident in different planes. (b) Willow-leaf dispersion figure for one incidence angle which corresponds to $\Delta\Phi_R$ equal to $(180 \pm 40)°$ within the frequency band of relative width 20%. (c) First MS we have studied with the aim to obtain the willow-leaf dispersion figure – the so-called mushroom structure. The black circles in the point out the vias, the black bars are switchable capacitive loads. (d) 3D view of the group of meta-atoms – Jerusalem crosses connected by switchable capacitive loads.

with a rather low permittivity. The willow-leaf dispersion figure with angular and polarization stability (insets) up to the angle $\theta_{max} = 45°$ was theoretically obtained for it. In Fig. 2(b) we show the dispersion figure in the scale which allows one to inspect $\Delta\Phi_R$. We see that $\Delta\Phi_R$ is equal to $(180 \pm 40)°$ (the target value and bounds are shown by horizontal lines) within the frequency band of relative width 20%. Our MS is a kind of high-impedance surface (see e.g. in [50]) whose grid is self-resonant, though at the resonance frequencies $\omega_{01,02}$, it operates in the capacitive regime.

Not every high-impedance surface may offer such a result. We started our investigation with the analysis of the most popular microwave high impedance surface called the mushroom-field MS or simply the mushroom structure. A body of literature is dedicated to the advantages of mushroom structures, their numerous applications, and specific features which can be engineered in these structures via variation of the design parameters (see e.g. in [43], [44], [45], [46], [47], [48], [49], [50], [51], [52], [53]). In the mushroom structure, the top grid is an array of small patches connected to the ground plane by vias piercing the substrate. However, in the next subsection, we show that this structure is in principle not suitable to achieve the goal of the present paper. Then we show that the proposed grid of Jerusalem crosses grants the needed properties if its parameters are properly chosen (the details are in Appendix). We try to answer the question whether it is possible to replace a group of our meta-atoms (Jerusalem crosses) with a single element with resonant sizes i.e. is it possible to transit from the MS to the MG? We do not give the final answer since our best result for the MG is much worse than that offered by our MS. In this paper, we verify the results of our analytical model by full-wave numerical simulations and experimental measurements in which the agreement is excellent.

B. THE MUSHROOM-FIELD METASURFACE

In the mushroom structure, the period a is much smaller than λ, and the thickness h of the substrate is of the same order as the period or smaller. The gap between the patches is as a rule much smaller than the period ($g \ll a$). The loading can be performed by lumped capacitors connecting the adjacent patches.

According to [46], the grid impedance of an array of the square patches located on the dielectric susbtrate for TE and TM cases, respectively, is as follows:

$$Z_g{}^{TM} = -j\frac{\eta_{eff}}{2\alpha}, \quad Z_g{}^{TE} = -j\frac{\eta_{eff}}{2\alpha\left(1 - \frac{\sin^2\theta}{2\varepsilon_{eff}}\right)}. \tag{10}$$

In equations (10), ε_{eff} is the effective permitivity value of the uniform host medium, η_{eff} is the wave impedance of the host medium, and α denotes the grid parameters and for square array of patches can be obtained as:

$$\varepsilon_{eff} = \frac{\varepsilon_r + 1}{2}, \eta_{eff} = \sqrt{\mu_0/\varepsilon_0\varepsilon_{eff}},$$
$$\alpha = \frac{k_{eff}\,a}{\pi}\ln\left(\frac{1}{\sin\left(\frac{\pi g}{2D}\right)}\right) \tag{11}$$

Period a and gap g are shown in Fig. 2, k_{eff} is the wave vector of the host medium and equals to $k_{eff} = k_0\sqrt{\varepsilon_{eff}}$. The loading capacitance C_l connected each pair of the adjacent patches and is simply added to the effective capacitance of the unloaded grid [52]. The last one can be easily retrieved from (10) because α is proportional to ω.

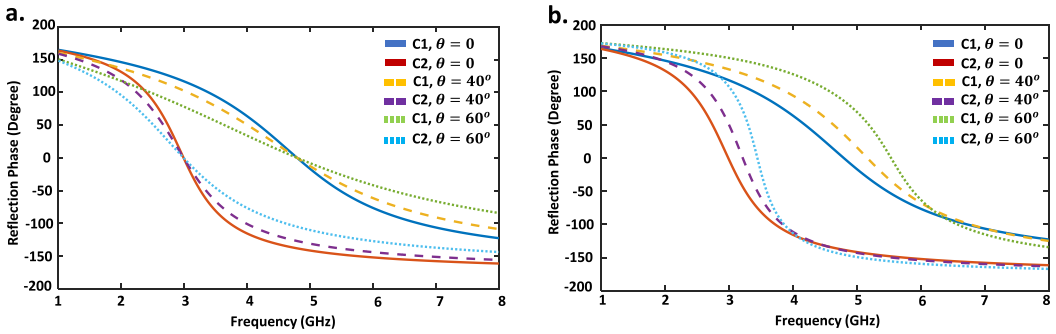

FIGURE 3. Analytical simulation of the willow-leaf dispersion for a mushroom structure with low permittivity substrate when the structure is illuminated by (a) TM and (b) TE polarized waves.

The surface impedance Z_- of the substrate is calculated involving the theory of so-called the wire medium or wire metamaterial sandwiched between the patch array and the ground plane. Usually, these wires (vias) are very thin and in the TE case (electric field is orthogonal to these wires) do not interact with the wave refracted into the substrate. Then for any incidence angle, we may write (see e.g. [50]):

$$Z_{s-}{}^{TE} = j\omega\mu_0 h. \tag{12}$$

For the TM polarized waves, the situation is different. Let us first consider the metal-backed substrate in the absence of the vias. Then, in accordance to [46], we have:

$$Z_-{}^{TM} = j\omega\mu_0 h\left(1 - \frac{\sin^2\theta}{\varepsilon_r}\right). \tag{13}$$

Since Z_g^{TM} does not depend on θ, the angular dependence of Z_s^{TM} cannot be compensated and the angular stability of the resonance is achieved only if $\varepsilon_r \gg 1$. In the presence of the vias we achieve the angular stability of the resonance for all angles, because in accordance to [46], we have:

$$Z_-{}^{TM} = j\omega\mu_0 h. \tag{14}$$

On the other hand, for the TE case, the angular stability of the resonance can be achieved if $\varepsilon_{eff} \gg 1$. What does this angular stability demand for ε_r? How this is compatible with the requirement of the modest slope of the RPFD? In order to understand it, we performed the calculations of RPFD of mushroom structures for different values of the permittivity and different sets of design parameters. In order to broaden the resonance band, we assumed that the dielectric substrate is lossy. The result for the dispersion figure is closest to the target willow-leaf shape for the following set of parameters: $\varepsilon_r = 2$(1-j0.2), $a = 5$mm, $g = 0.1$mm and $h = 6$mm. The analytically calculated reflection phase diagram of the structure for the TM field is depicted in Fig. 3(a). Here the incidence angle varies up to 60° and the angular stability is achieved. For all θ up to 60°, we have $140° < \Delta\Phi_R < 220°$ in the band of frequencies broader than 20%. The two states of the pin diode needed to create the willow-leaf shape are set as $C_1 = 0$ (when the grid capacitance is that between the adjacent patches) and $C_2 = 0.23$ pF.

Meanwhile, the result for the TE case presented in Fig. 3(b) shows the noticeable shift of both resonances even for $\theta = 20°$. Though the low value of the substrate permittivity offers the willow-leaf shape for all angles, the angular stability is not achievable in the TE case even for a narrow band of frequencies. We do not report the full-wave simulations confirming these analytical calculations, because the reliability and very high accuracy of the used analytical model have been validated theoretically and experimentally in the already cited works.

The angular stability of the dispersion curve is possible with the high permittivity for the mushroom structure, but the willow-leaf shape will be lost. Fig. 4(a-c) depicts the reflection phase dispersion of the mushroom structure with the same geometrical parameters as above illuminated by TE polarized waves. Three different values of the substrate relative permittivity were chosen to show the evolution of the RPFD versus both incidence angle and permittivity. By increasing the permittivity, we stabilize the resonance frequency but the resonance becomes too narrow-band and the willow-leaf dispersion figure becomes impossible.

The best result of our extensive analytical simulations of the mushroom structures is presented in Fig. 5. It corresponds to the rather high substrate permittivity ε_r=9(1-j0.02), when $C_1 = 0$ and $C_2 = 0.38$ pF. The other parameters are the same as above for a fair comparison. The criterion for $\Delta\Phi_R$ for the non-polarized incident wave is fulfilled only in the range 2.2-2.4 GHz (8.5% relative bandwidth instead of 20%). We have concluded that for the mushroom structures the angular stability of the TE-polarized reflection phase is not compatible with the broadband operation.

C. THE GRID OF JERUSALEM CROSSES ON TOP OF A METAL-BACKED SUBSTRATE

The analytical model of the MS we have proposed as a binary RIS was developed in work [54]. The angular stability of this MS was not studied in [54], and in this paper we do it. According to [54], the grid impedance of the planar array of Jerusalem crosses in the case of a small gap g between them can be calculated, for the TM and TE incident waves,

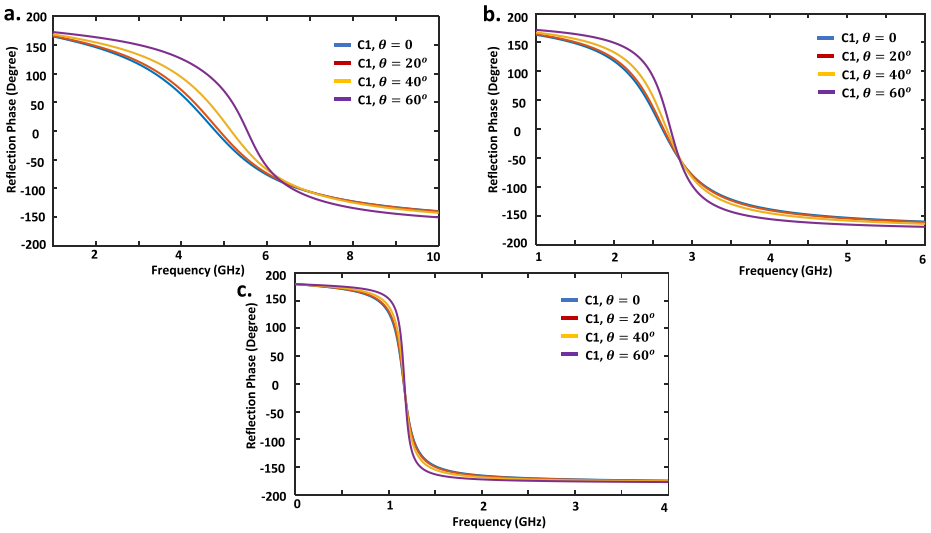

FIGURE 4. One-state ($C_1 = 0$) RPFD for the mushroom structure for three values of the substrate permittivity: (a) ε_r=2, (b) ε_r=9(1-j0.02), (c) ε_r=50(1-j0.002) in the TE incidence case. The resonance is not robust with respect to θ in (a,b) and is robust but narrow-band in (c).

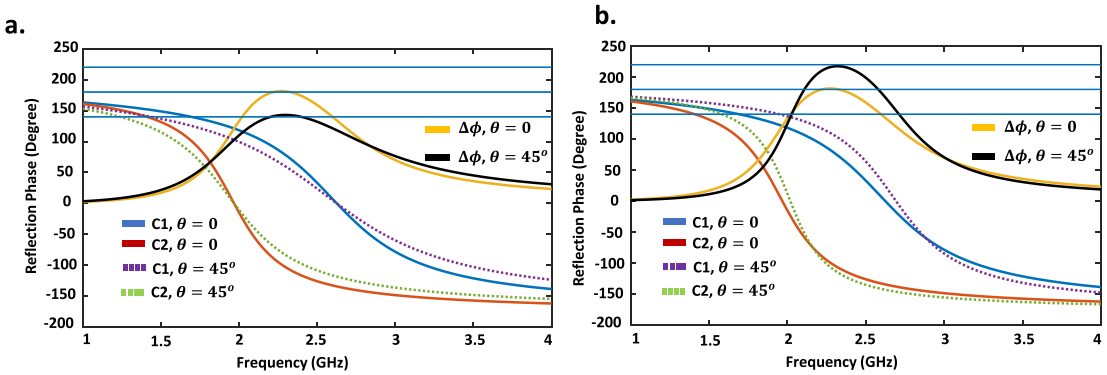

FIGURE 5. Willow-leaf dispersion figure and $\Delta\Phi_R$ for the mushroom structure with the permittivity of the substrate ε_r=9(1-j0.02), when the structure is illuminated by (a) TE and (b) TM polarized waves. Horizontal lines show the target value of $\Delta\Phi_R$ and its allowed bounds.

respectively, as follows:

$$Z_g{}^{TM} = j\frac{\eta_{eff}\alpha}{2}\left(1-\frac{\sin^2\theta}{2\varepsilon_{eff}}\right)+\frac{1}{j\omega C_g},$$
$$Z_g{}^{TE} = j\frac{\eta_{eff}\alpha}{2}+\frac{1}{j\omega C_g} \quad (15)$$

Here α is the parameter of the grid of strips calculated in accordance to (11) with the replacement $g \to w$ (w is the strip width), C_g is the sum of the effective capacitance of the unloaded grid C_{eff}, and the capacitance of the pin diode C_l. The effective capacitance of the grid C_{eff} takes into account the interaction between all elements of the crosses [55]:

$$C_{eff} = \frac{2}{\pi}\varepsilon\varepsilon_0 d\left[\log cosec\left(\frac{\pi g}{2a}\right)+F\right], \quad (16)$$
$$F = \frac{Qu^2}{1+Q(1-u)^2}+\left(\frac{du\,(3u-2)}{4\lambda_{eff}}\right)^2$$
$$Q = \sqrt{1-\left(\frac{d}{\lambda_{eff}}\right)^2}, \quad u = \cos^2\frac{g\pi}{2d}, \quad \lambda_{eff} = \frac{2\pi}{k_{eff}} \quad (17)$$

Parameters d, g, w as well as the period a are shown in Fig. 2(d).

We see that Z_g is independent of θ in the TE case. In the TM case Z_g depends on θ, however, in the Appendix we show that this dependency in the dispersion equation cancels out with the angular dependency of the substrate. The approximate parallelism of the '0' state RPFD to the '1' state RPFD is ensured by the capacitive impedance of the grid at the resonance frequency (see above). The modest slope of the RPFD is granted by the broad resonance band for $\varepsilon_r \ll 10$. The study of the angular stability of the resonance frequency for an arbitrary load is presented in Appendix. The presence of the vertical vias in the substrate is not needed for the angular stability of RPFD. Both analytical and full-wave simulations confirmed that vertical vias, in this case, would be only harmful.

Fig. 6 shows the analytical simulations of the willow-leaf figure for several incidence angles in the TE case, and Fig. 12 shows the corresponding results for the TM case. The parameters of our MS are as follows: period $a = 5$ mm,

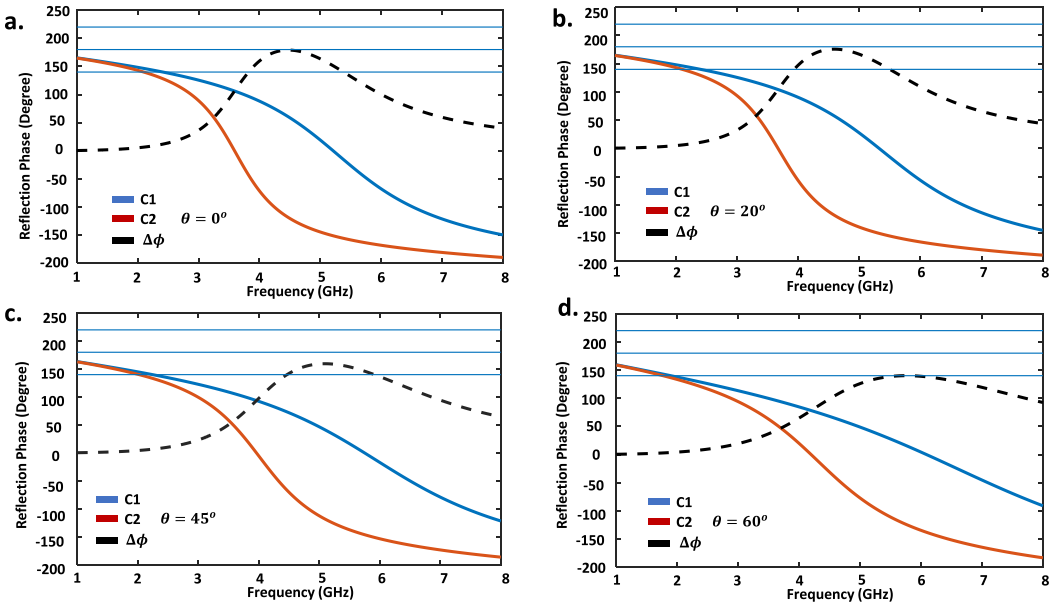

FIGURE 6. The two-states RPFD of our RIS and phase difference $\Delta\Phi_R$ in the TE case for (a) θ =0, (b) $\theta = 20°$, (c) $\theta = 45°$ and (d) $\theta = 60°$.

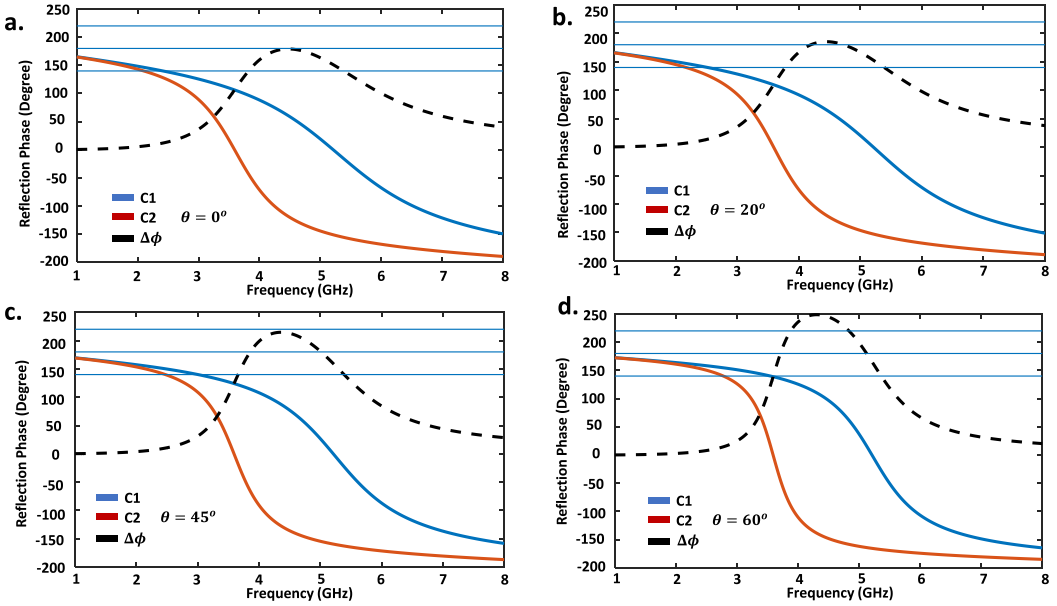

FIGURE 7. The two-states RPFD of our RIS and $\Delta\Phi_R$ in the TM case for (a) θ =0, (b) $\theta = 20°$, (c) $\theta = 45°$ and (d) $\theta = 60°$.

length of the strip $d = 2$ mm, strip width $w = 0.2$ mm, and gap between the crosses $g = 0.1$ mm. For a fair comparison to the mushroom structure, we have selected the same substrate of the thickness of $h = 6$ mm. Then the operation band is close to that of the mushroom-field MS. The two states of the lumped element were set as $C_1 = 0$ and $C_2 = 100$ fF. A so small loading capacitance is an advantage of our structure. Using available switches based on pin-diodes, one may easily obtain the loading capacitance of this magnitude in the ON state and zero capacitance in the OFF state, whereas the parasitic losses and inductances will be negligibly small [58].

Referring to phase differences (black dotted lines) depicted in Figs. 6(a-c) and 7(a-c), our criteria of the operation bandwidth in which $140° < \Delta\Phi_R < 220°$ are fulfilled up to $\theta = 45°$ for both polarizations. Similar results can be shown for other sets of the design parameters and different frequency ranges if we respect the condition $\varepsilon_r \ll 10$.

To validate our analytical results, we performed extensive full-wave numerical simulations using CST Microwave Studio (version 2020). We utilized the Floquet solver with periodic boundary conditions in the grid plane, whilst an open boundary condition is applied along the normal. For the aforementioned set of design parameters the willow-leaf

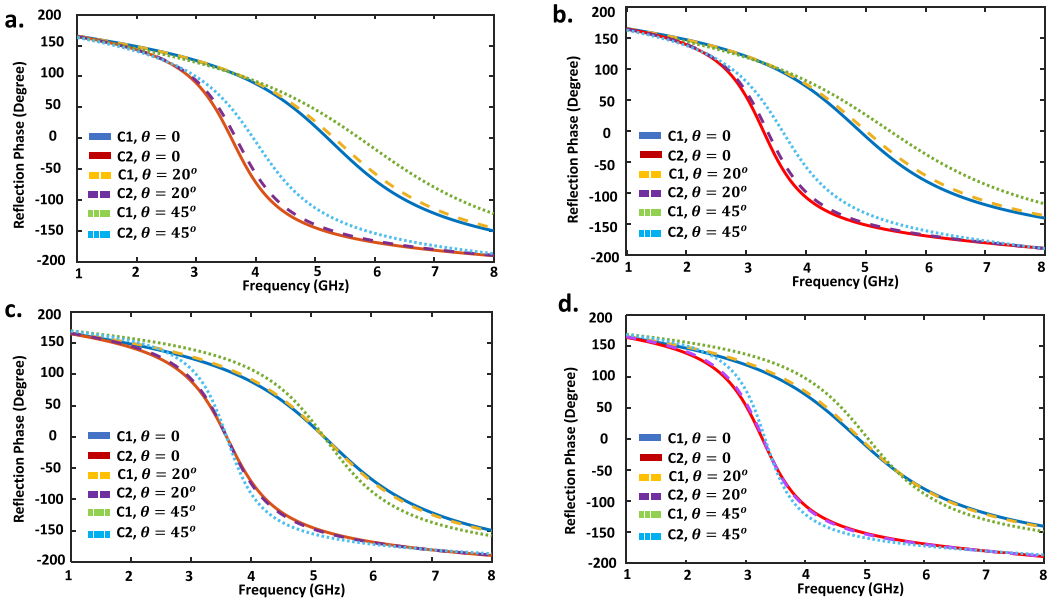

FIGURE 8. Comparison between analytical (Matlab) and full-wave (CST) simulations of the willow-leaf shapes for our RIS: (a) analytical TM case, (b) full-wave TM case, (c) analytical TE case, (d) full-wave TE case.

dispersion shapes simulated in both Matlab and CST are presented in Fig. 8. The incidence angle varies in these simulations from 0 to 45° degrees for both incident wave polarizations. The agreement between our analytical calculations and full-wave simulations is excellent. In general, the accuracy of our analytical model validated by full-wave simulations turned out to be surprising.

D. DISCUSSION

In this paper, we have suggested and theoretically studied the broadband RIS which operates in the binary regime for a wide range of incidence angles and both polarizations of the incident wave. The RIS is performed as an MS loaded by pin-diodes. The MS can be fabricated using only planar technology since the substrate does not comprise vias. The size of the unit cell at the central frequency of the operation band is as small as $a = \lambda/12$.

A question remains whether it is possible to replace a group of unit cells in the same state '0' or '1' occupying one half of the period D of a periodical RIS by a single scattering element i.e. is it possible to transit from the MS to the MG. We have studied this issue and did not find a suitable MG. When the horizontal dimensions of the scattering element of the top grid approach $\lambda/2$, its resonance band becomes dependent on θ and different for the TE and TM cases. The angular and polarization stability was achieved for an array of resonant patches [56], [57] sufficiently distanced from one another, however, it was achieved only in a narrow frequency band. Fig. 9(a) sketches the 3D view of 2×2 unit cells. The unit cell size is close to $\lambda/2$ in the range $2.1 - 2.5$ GHz, whereas the patch size, a equals the gap between the patches and is close to $\lambda/2$. For a fair comparison, the substrate material and thickness h were chosen the same as those in our RIS, i.e. Arlon AD255C, $h = 6$ mm. The two states resulted from the loading capacitance $C_2 = 43$ fF, whereas $C_1 = 0$. In 9(b-d) we show the phase difference $\Delta\Phi_R$ for three incident angles: $\theta = 20°$, $\theta = 35°$ and $\theta = 45°$. For $\theta = 20°$ the criterion of the broadband operation is approximately satisfied: the phase difference is in the target range $140° < \Delta\Phi_R < 220°$ in the band of a relative with near 18%. However, for $\theta = 35°$ this band shrinks to 10%, and for $\theta = 45°$ the structure does not work. Thus, our criteria of operation are not fulfilled.

To our opinion, the advantage of the MS compared to the MG in what concerns the angular stability is the different nature of the resonance. In the MS the capacitive top grid resonates with the inductive substrate. The angular dependence of the grid reactance can be compensated by the angular dependence of the substrate inductance. In the MG every patch is a cavity resonator [56], [57] and we do not see how to compensate for the angular dependence of its resonance.

IV. FABRICATION AND MEASUREMENTS

To validate the performance and precision of our proposed method, a prototype array of 37×37 unit cells is fabricated to mimic the periodic boundary conditions in our full-wave simulations. The total size of the prototypes is $296 \times 296\, mm^2$ (Fig. 10(b)). Our proposed angle and polarization-insensitive RIS is composed of a grid of Jerusalem crosses on top of a metal-backed substrate. We have to change the capacitance between each adjacent grid so that a phase difference is guaranteed for a broad range of our interest frequency. It is possible to achieve this phase difference either by changing the capacitance of the pin diodes or by changing the structural capacitance. Because of the ease in fabrication

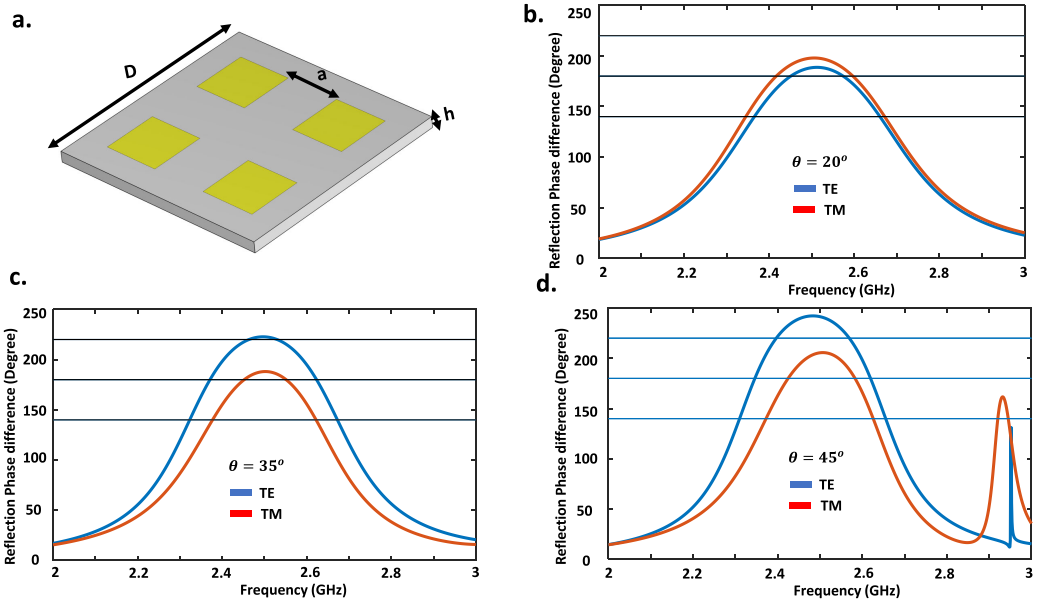

FIGURE 9. a) 3D view of four unit cells of the meta-grating-based RIS. the geometrical parameters are as follows: period D=60mm, patch size and the gap between the patches $a = 30$ mm, substrate thickness $h = 6$ mm. (b)-(d) Full-wave simulations of $\Delta\Phi_R$ for both TE (blue curves) and TM (red curves) cases, whereas θ is equal to (b) $\theta = 20°$, (c) $\theta = 35°$ and (d) $\theta = 45°$.

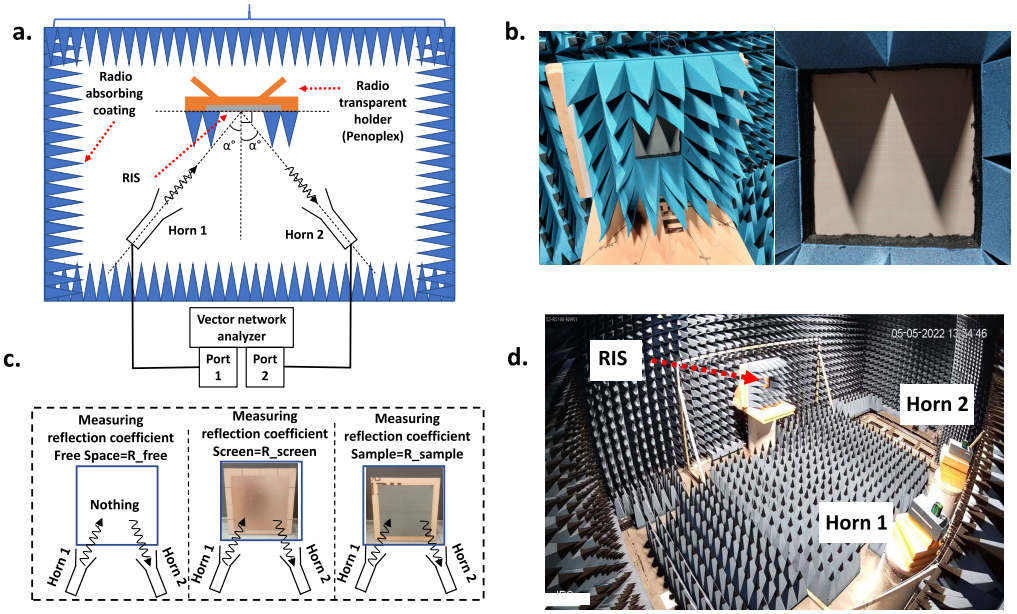

FIGURE 10. (a) Schematic view of the measurement setup in the anechoic chamber for evaluating the RIS phase response. (b) Photo of the fabricated RIS prototype. (c) Demonstration of three sets of measurment for each incident angle and polarization. (d) 3D view of the experimental setup.

and the tolerance between the nominal capacitance values of pin diodes (as well as the disparities between their actual value and their circuit model value), we designed two RISs with different structural capacitances. The geometrical parameters of the RISs are as follows: *RIS*_1 (a=8mm, d=4mm, g=0.2mm, and w=0.2mm), and *RIS*_2 (a=8mm, d=1mm, g=0.5mm, and w=0.2mm). The substrate is Arlon AD255C with relative permittivity ε_r=2.6(1-j0.0014) and thickness of h=1.016mm. Due to our fruitful investigation in the Appendix, a lower value of substrate permittivity results in a broader range of operation for our willow-leaf figures. In line with our investigation, we use an air gap equal to 7mm between the substrate and ground plane. Now, our RIS can work between 4.7-6.5 GHz (32% of a frequency band) when the incident angle changes up to $\theta = 45°$ degrees under dual-polarized waves (see Fig. 11).

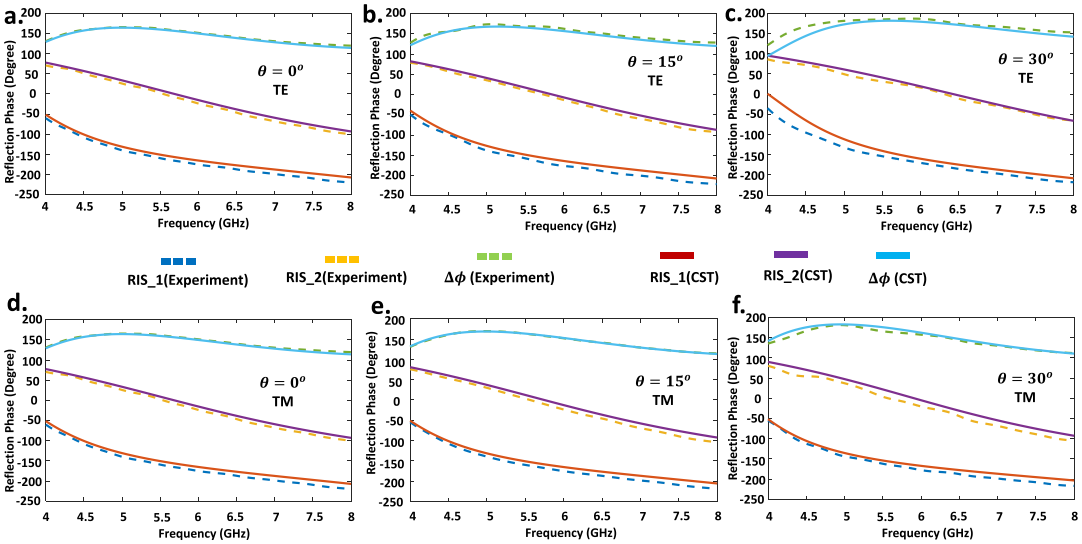

FIGURE 11. Comparison between CST full wave and measurement results of the two-states RPFD of our fabricated RISs (*RIS*_1, and *RIS*_2) and phase difference $\Delta\Phi_R$ from 4-8 GHz in TE case for (a) $\theta = 0°$, (b) $\theta = 15°$ and (c) $\theta = 30°$. The results for the TM case are presented in (d-f) when the incident angle equals to (d) $\theta = 0°$, (e) $\theta = 15°$ and (f) $\theta = 30°$.

Fig. 10 shows the measurement setup and fabricated prototype. To prevent any possible interference from the environment, the measurements were performed in a microwave anechoic chamber (Fig. 10(d)) using a vector network analyzer (VNA, Rohde & Schwarz ZVB 20), and two linearly polarized horn antennas covering the frequency range of 4 to 8 GHz. The schematic demonstration of the measurement setup is depicted in Fig. 10(a). To fulfill Floquet port excitation, the transmitting and receiving horn antennas were carefully adjusted symmetrically on both sides of the normal axis of the RIS with the angle of $\alpha°$. The distance between the sample and antennas is set 4.25 meters to guarantee a quasi-plane wave excitation. Due to the restrictions of our experimental setup, for extreme incident angles, most of the transmitted power would be absorbed by the Radio absorbing coating. Therefore, the measurements have been done for three incident angles of $\theta = 0$, $\theta = 15°$, and $\theta = 30°$. For each incident angle and each linear polarization, three measurements were done including the reflection coefficient without our sample, reflection coefficient with the screen, and reflection coefficient with the sample. Then using the time gating method [59], the results have been converted. Next, by using a direct Fourier transform of the converted results and normalization to the result of the free space measurement, the true reflection coefficients versus frequency were obtained.

In Fig. 11, the solid lines and dashed lines represent the results of the CST simulations and the experiment respectively. As can be observed, the simulated and measured willow-leaf dispersion figures, as well as phase differences, are in a good agreement. The finite size of our sample did not result in a disagreement thanks to the subwavelength size of the proposed unit cell ($a \approx \lambda/7$), that made our sample in its absorbing surround operating similarly to an infinite array illuminated by a plane wave. Eventually, the angular and polarization insensitivity of our proposed RIS in a broad range of frequencies (32% of bandwidth) is validated through simulations and measurements which proves the effectiveness of the proposed theoretical analyses.

V. CONCLUSION

In summary, in this paper, we have solved analytically the problem of the angular instability of a binary RIS operating in a broadband regime. We started our solution from the formulation of the target shape of the two-states reflection phase-frequency dispersion that we called it as the willow-leaf figure. This figure should be robust with respect to the variation of the incidence angle. We have shown that for all incidence angles for the TE-polarization of the incident wave it is impossible. However, for the angular range $-45° \leq \theta \leq +45°$ it is possible to achieve the robust operation for both TE and TM cases in the frequency band of 20% relative width. Conventional metasurfaces such as mushroom structures are not suitable for this. We also did not manage to attain the goal with a meta-grating of resonant patches. But the grid of Jerusalem crosses on top of a thin metal-backed dielectric substrate granted the needed frequency and angular behavior for both polarizations of the incident wave. The binary operation is offered by pin diodes connecting the adjacent crosses and changing the structural capacitance. Full-wave simulations have shown the excellent agreement with the analytical model. Finally, by performing a set of measurements, the angular and polarization stability of our proposed RIS in a broad range of frequency band was verified.

The advantage of our MS is its simplicity – unlike mushroom structures, there are no vias. It makes our MS promising for scaling to the mmWave range via proportional reduction of all dimensions. In the present paper, we reported the microwave calculations only because the experiment

in the microwave range is simpler than the mmWave experiment and we plan to do it prior to engineering the mmWave RIS.

We plan to study how our MS deflects the realistic wave beam. Recall, that we assumed the reflective properties of a big group of our unit cells to be the same as those of the infinite uniform MS that we have studied above. This assumption allowed us to use the periodic boundary conditions. In the next stage, we will consider the anomalous reflection of our MS in the binary regime when the period D of the loading is given by (1). Then this assumption will be validated.

We believe that leveraging our technique will meet the prospective industrial demands and will be helpful in the embodiment of ''smart radio environment'' of the near future.

APPENDIX 1

In this Appendix, we prove that a self-resonant grid of Jerusalem crosses on a thin metal-backed dielectric layer manifests the angular stability of the resonance frequency for both polarizations of the incident waves.

From (2) we obtain formulas valid for both TE and TM cases:

$$r_s = \frac{(r_g r_- - X_g X_-)r_\Sigma + (r_g X_- + X_g r_-)X_\Sigma}{r_\Sigma^2 + jX_\Sigma^2}, \quad (18)$$

$$X_s = \frac{(X_g X_- - r_g r_-)X_\Sigma + (r_g X_- + X_g r_-)r_\Sigma}{r_\Sigma^2 + jX_\Sigma^2} \quad (19)$$

Eq. (19) implies the resonance at the frequency ω_0 which satisfies to:

$$(X_g X_- - r_g r_-)(X_g + X_-) + (r_g X_- + r_- X_g)(r_g + r_-) = 0 \quad (20)$$

In general, this equation does not reduce to $(X_g + X_-) = 0$ as it is adopted in the theory of high-impedance surfaces (see e.g. in [50]). Only if the resonance band is narrow i.e. when both R_g and R_- are very small, Eq. (20) really yields to $(X_g + X_-) = 0$. However, this is not our case. The modest slope of the RPFD implies the broad resonance band of the targeted MS. We need a modest slope of RPFD that demands the modest values of both $X_g(\omega_0)$ and $X_-(\omega_0)$. It means that we cannot neglect $r_{g,-}$ compared to $X_{g,-}$ in the equation (20). This is the reason why the θ-dependent terms of the grid impedance Z_g and of the metal-backed substrate impedance, Z_- may enter into the resonance equation with opposite signs.

Adopting that the dielectric losses in our MS dominate over the Ohmic losses, we consider the metal grid as perflectly conducting and take into account the loss tangent of the substrate, assuming $\varepsilon_r = \varepsilon' - j\varepsilon''$, where $\varepsilon' \gg \varepsilon''$.

For the grid impedance of the Jerusalem crosses and for the surface impedance of the substrate in the TE-case we have:

$$Z_g^{TE} = \frac{j\eta\alpha}{2} + \frac{1}{j\omega_0 C_g}, \quad Z_-^{TE} = r_- + j\omega_0\mu_0 h. \quad (21)$$

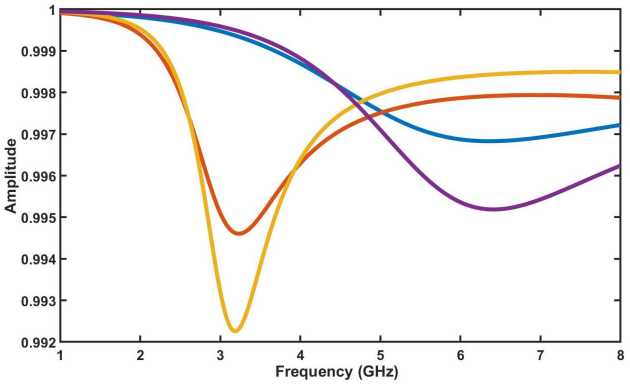

FIGURE 12. The magnitude of the two states of willow-leaf figures for normal and $\theta = 45°$.

Here the first formula reproduces (15) and the second formula results from the dielectric loss:

$$r_- = \varepsilon''\mu_0\omega h\frac{(kh)^2}{3}. \quad (22)$$

This relation is absent in the theory of our MS [54], but it follows from formula (7) of [54] if we apply the Taylor expansion to the function $\tan(K_z h)/K_z$ entering that formula. Here, K_z is the normal component of the refracted wave vector in the substrate, and $|K_z h| \ll \pi/2$, because the substrate is thin and its permittivity is low. Since θ does not enter our formulas we see that the metasurface based on Jerusalem crosses has no problem with angular stability of the resonance for the TE-polarization case.

For the TM-case we have to take into account the dielectric loss when we calculate the grid impedance:

$$X_g^{TM} = \frac{\eta\alpha}{2}\left(1 - \frac{\sin^2\theta}{\varepsilon' + 1}\right) - \frac{1}{\omega C_g} \quad (23)$$

$$r_g^{TM} = \frac{\eta\alpha}{2}\frac{\varepsilon''\sin^2\theta}{\varepsilon' + 1} \quad (24)$$

The surface impedance of the grounded substrate can be calculated as [54]:

$$Z_-^{TM} = j\omega\mu_0\frac{\tan K_z h}{K_z}\left(1 - \frac{\sin^2\theta}{\varepsilon}\right) \quad (25)$$

which results in the following relations for the reactance and resistance of the substrate:

$$X_-^{TM} = \omega\mu_0 h\left(1 - \frac{\sin^2\theta}{\varepsilon'}\right) \quad (26)$$

$$r_-^{TM} = \omega\mu_0 h\varepsilon''\left[\frac{(kh)^2}{3}\left(1 - \frac{\sin^2\theta}{\varepsilon'}\right) + \frac{\sin^2\theta}{\varepsilon'}\right] \quad (27)$$

Since $(kh)^2 \ll 1$, expression (27) can be simplified and takes the form

$$r_-^{TM} = r_- + \omega\mu_0 h\varepsilon''\frac{\sin^2\theta}{\varepsilon'}, \quad (28)$$

where r_- is given by (22). Let the dielectric constant ε' be not very high, e.g. lies in the limits $\varepsilon' = 2 - 4$. Then for

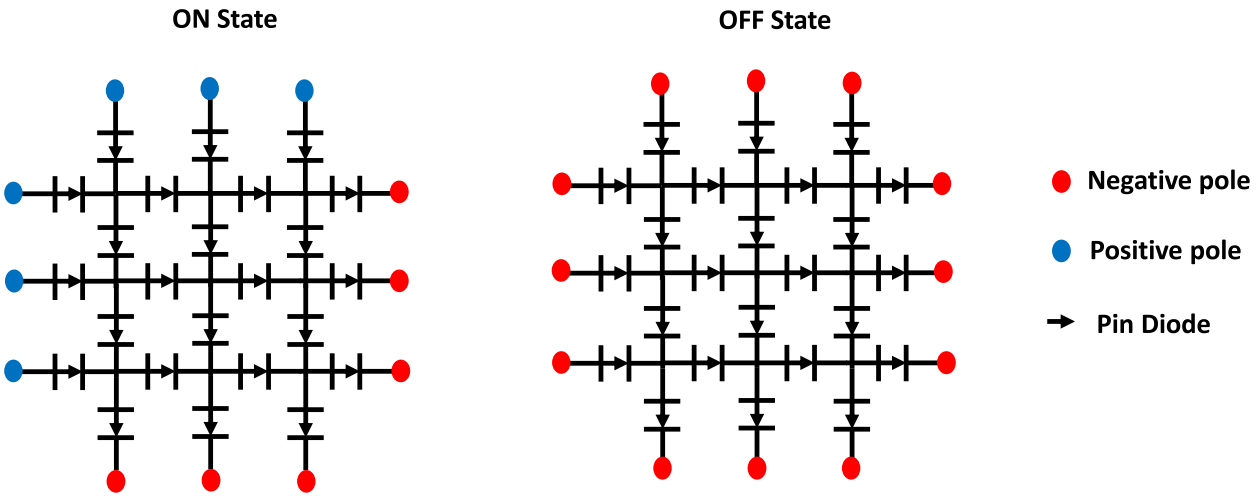

FIGURE 13. The schematic view of the approach for biasing the grid of Jerusalem crosses.

the small incidence angles satisfying $\sin^2\theta < (kh)^2\varepsilon'/3$ the resonance frequency cannot be noticeably different from that corresponding to $\theta = 0$ simply because these angles are very small. Now, consider the moderate angles which are sufficiently large so that to write for them $\sin^2\theta \gg (kh)^2\varepsilon'/3$. For these angles (28) evidently reduces to

$$r_-^{TM} = \omega\mu_0 h\varepsilon''\frac{\sin^2\theta}{\varepsilon'} \tag{29}$$

Introducing notations

$$\xi_0 = \frac{\eta\alpha}{2\omega}, \quad \xi_1 = \frac{\xi_0}{\varepsilon'+1}, \quad \psi_0 = \mu_0 h, \quad \psi_1 = \frac{\psi_0}{\varepsilon'},$$

we may rewrite formulas (23), (24), (26) and (29) as

$$X_g^{TM} = \xi_0\omega - \frac{1}{\omega C_g} - \xi_1\omega\sin^2\theta \tag{30}$$

$$r_g^{TM} = \varepsilon''\xi_1\omega\sin^2\theta, \tag{31}$$

$$X_-^{TM} = \psi_0\omega - \psi_1\omega\sin^2\theta, \quad r_-^{TM} = \varepsilon''\psi_1\omega\sin^2\theta. \tag{32}$$

Substituting expressions (30), (31) and (32) into Eq. (20), we obtain an equation

$$\left((\xi_0 - \xi_1\sin^2\theta)\omega - \frac{1}{\omega C_g}\right)\left[\left((\xi_0 - \xi_1\sin^2\theta)\omega - \frac{1}{\omega C_g}\right)\right.$$
$$\times(\psi_0 - \psi_1\sin^2\theta)\omega + (\psi_0 - \psi_1\sin^2\theta)^2\omega^2 + \frac{\psi_1\omega\sin^2\theta}{\omega^2 C_g^2}$$
$$\left.-(\varepsilon'')^2(\xi_1^2 + \psi_1^2)\cdot\omega^2\sin^4\theta\right] - (\varepsilon'')^2(\xi_1^2 + \psi_1^2)$$
$$\times(\psi_0 - \psi_1\sin^2\theta)\omega^3\sin^6\theta = 0 \tag{33}$$

The terms proportional to $\sin^2\theta$ and $\sin^4\theta$, enter this equation with different signs. They cancel out (for both $\sin^2\theta$ and $\sin^4\theta$) on condition $\psi_1 = \xi_1$ (terms with C_g cancel out automatically). Note that condition $\psi_1 = \xi_1$ simultaneously equates r_g to r_- and the angle-dependent part of X_g to that of X_-.

In fact, in (33) there are also terms proportional to $\sin^6\theta$ and $\sin^8\theta$ which do not cancel out. However, for $\varepsilon' > 2$ and $\theta \le \pi/4$ these terms can be neglected. Thus, an approximate condition of the angular stability of resonance frequency for sufficiently small θ can be written in the form

$$\varepsilon' a\log\frac{2a}{\pi w} = \pi(\varepsilon'+1)h \tag{34}$$

This condition is respected in our design solution. Notice, that our result is valid only for moderate values of ε'. If $\varepsilon' \ge 5-10$, the angles satisfying to the condition $\sin^2\theta < (kh)^2\varepsilon'/3$ are not small and we cannot be sure a priori that the resonance for these incidence angles is the same as for $\theta = 0$. Moreover, for these angles r_g cannot be equated to r_- i.e. we cannot achieve the compensation of the angle-dependent terms in (20) and the angular stability of the resonance frequency for the TM case will be not possible.

APPENDIX 2

In this Appendix, we will show the amplitude profiles of the two states of willow-leaf figures for normal and $\theta = 45°$. For the ON state, the resistance of the pin diode is considered 7 ohms while for the OFF state it is negligible and equal to zero. Based on the simulation results, the reflection from the metasurface is above 0.99 which shows the perfect reflectivity of our surface.

APPENDIX 3

This Appendix shows the potential method of biasing the grid of Jerusalem crosses for our uniform metasurface. Noted that our structure was not reconfigurable, but by inserting pin diodes it can be tunable. As depicted in Fig. 13 the biasing may be done with a simple configuration. The blue and red color spots show the connections of the positive and negative poles. This biasing scheme does not need any vias. For the ON state, the voltage should be applied to the positive poles. Since the capacitances of the pin diodes have a series connection, a small amount of voltage is enough to turn the diodes ON. On the other hand, for the OFF state, there is no need to

apply a voltage. This simple configuration allows our uniform metasurfaces to work as a tunable device between two states.

ACKNOWLEDGMENT

The authors acknowledge Stanislav Glybovski and Danil Vabischevich for important technical help.

REFERENCES

[1] M. Z. Chowdhury, M. Shahjalal, S. Ahmed, and Y. M. Jang, "6G wireless communication systems: Applications, requirements, technologies, challenges, and research directions," *IEEE Open J. Commun. Soc.*, vol. 1, pp. 957–975, 2020.

[2] P. Yang, Y. Xiao, M. Xiao, and S. Li, "6G Wireless communications: Vision and potential techniques," *IEEE Netw.*, vol. 33, no. 4, pp. 70–75, Jul./Aug. 2019.

[3] L. Feng, X. Que, P. Yu, W. Li, and X. Qiu, "IRS assisted multiple user detection for uplink URLLC non-orthogonal multiple access," in *Proc. IEEE Conf. Comput. Commun. Workshops (INFOCOM WKSHPS)*, Jul. 2020.

[4] W. Tang, X. Chen, M. Z. Chen, J. Yan Dai, Y. Han, M. D. Renzo, S. Jin, Q. Cheng, and T. J. Cui, "Path loss modeling and measurements for reconfigurable intelligent surfaces in the millimeter-wave frequency band," 2021, *arXiv:2101.08607*.

[5] W. Tang, "Wireless communications with reconfigurable intelligent surface: Path loss modeling and experimental measurement," *IEEE Trans. Wireless Commun.*, vol. 20, no. 1, pp. 421–439, Jan. 2021.

[6] H. Taghvaee, A. Jain, S. Abadal, G. Gradoni, E. Alarcón, and A. Cabellos-Aparicio, "On the enabling of multi-receiver communications with reconfigurable intelligent surfaces," 2021, *arXiv:2106.06789*.

[7] D. Wu, J. Wang, Y. Cai, and M. Guizani, "Millimeter-wave multimedia communications: Challenges, methodology, and applications," *IEEE Commun. Mag.*, vol. 53, no. 1, pp. 232–238, Jan. 2015.

[8] M. D. Renzo, F. H. Danufane, and S. Tretyakov, "Communication models for reconfigurable intelligent surfaces: From surface electromagnetics to wireless networks optimization," 2021, *arXiv:2110.00833*.

[9] M. D. Renzo, "Smart radio environments empowered by reconfigurable AI meta-surfaces: An idea whose time has come," *EURASIP J. Wireless Commun. Netw.*, vol. 2019, no. 1, pp. 1–20, 2019.

[10] E. Basar, M. D. Renzo, J. D. Rosny, M. Debbah, M. Alouini, and R. Zhang, "Wireless communications through reconfigurable intelligent surfaces," *IEEE Access*, vol. 7, pp. 116753–116773, 2019.

[11] Q. Wu and R. Zhang, "Towards smart and reconfigurable environment: Intelligent reflecting surface aided wireless network," *IEEE Commun. Mag.*, vol. 58, no. 1, pp. 106–112, Nov. 2020.

[12] G. Gradoni, "Smart radio environments," 2021, *arXiv:2111.08676*.

[13] M. Hua and Q. Wu, "Joint dynamic passive beamforming and resource allocation for IRS-aided full-duplex WPCN," *IEEE Trans. Wireless Commun.*, vol. 21, no. 7, pp. 4829–4843, Jul. 2022.

[14] J. Zhao, "Programmable time-domain digital-coding metasurface for nonlinear harmonic manipulation and new wireless communication systems," *Nat. Sci. Rev.*, vol. 6, no. 2, pp. 231–238, Nov. 2018.

[15] J. Y. Dai, W. Tang, L. X. Yang, X. Li, M. Z. Chen, and J. C. Ke, "Realization of multi-modulation schemes for wireless communication by time-domain digital coding metasurface," *IEEE Trans. Antennas Propag.*, vol. 68, no. 3, pp. 1618–1627, May 2020.

[16] S. Taravati and G. V. Eleftheriades, "Intelligent-metasurface-assisted full-duplex wireless communications," 2021, *arXiv:2105.09436*.

[17] S. Zhang and R. Zhang, "Capacity characterization for intelligent reflecting surface aided MIMO communication," *IEEE J. Sel. Areas Commun.*, vol. 38, no. 8, pp. 1823–1838, Aug. 2020.

[18] X. Mu, Y. Liu, L. Guo, J. Lin, and N. Al-Dhahir, "Exploiting intelligent reflecting surfaces in NOMA networks: Joint beamforming optimization," *IEEE Trans. Wireless Commun.*, vol. 19, no. 10, pp. 6884–6898, Oct. 2020.

[19] H. Rajabalipanah, "Asymmetric spatial power dividers using phase-amplitude metasurfaces driven by Huygens principle," *ACS Omega*, vol. 4, no. 10, pp. 14340–14352, 2019.

[20] F. Ghorbani, S. Beyraghi, J. Shabanpour, H. Oraizi, H. Soleimani, and M. Soleimani, "Deep neural network-based automatic metasurface design with a wide frequency range," *Sci. Rep.*, vol. 11, no. 1, pp. 1–8, Dec. 2021.

[21] F. Ghorbani, J. Shabanpour, S. Beyraghi, H. Soleimani, H. Oraizi, and M. Soleimani, "A deep learning approach for inverse design of the metasurface for dual-polarized waves," *Appl. Phys. A, Solids Surf.*, vol. 127, no. 11, pp. 1–7, Nov. 2021.

[22] A. Díaz-Rubio, V. S. Asadchy, A. Elsakka, and S. A. Tretyakov, "From the generalized reflection law to the realization of perfect anomalous reflectors," *Sci. Adv.*, vol. 3, no. 8, Aug. 2017.

[23] N. Yu, P. Genevet, M. A. Kats, F. Aieta, J.-P. Tetienne, F. Capasso, and Z. Gaburro, "Light propagation with phase discontinuities: Generalized laws of reflection and refraction," *Science*, vol. 334, no. 6054, pp. 333–337, Oct. 2011.

[24] S. Sun, Q. He, S. Xiao, Q. Xu, X. Li, and L. Zhou, "Gradient-index metasurfaces as a bridge linking propagating waves and surface waves," *Nature Mater.*, vol. 11, no. 5, pp. 426–431, May 2012.

[25] L. Shao, M. Premaratne, and W. Zhu, "Dual-functional coding metasurfaces made of anisotropic all-dielectric resonators," *IEEE Access*, vol. 7, pp. 45716–45722, 2019.

[26] J. Shabanpour, "Implementation of conformal digital metasurfaces for THz polarimetric sensing," *OSA Continuum*, vol. 4, no. 4, pp. 1372–1380, 2021.

[27] J. Shabanpour, "Real-time multi-functional near-infrared wave manipulation with a 3-bit liquid crystal based coding metasurface," *Opt. Exp.*, vol. 29, no. 10, pp. 14525–14535, 2021.

[28] H. Rajabalipanah, A. Abdolali, J. Shabanpour, A. Momeni, and A. Cheldavi, "Addition theorem revisiting for phase/amplitude-encoded metasurfaces: Asymmetric spatial power dividers," 2019, *arXiv:1901.04063*.

[29] T. J. Cui, M. Q. Qi, X. Wan, J. Zhao, and Q. Cheng, "Coding metamaterials, digital metamaterials and programmable metamaterials," *Light, Sci. Appl.*, vol. 3, no. 10, pp. e218–e218, Oct. 2014.

[30] W. Tang, J. Y. Dai, M. Chen, X. Li, Q. Cheng, S. Jin, K.-K. Wong, and T. J. Cui, "Programmable metasurface-based RF chain-free 8PSK wireless transmitter," *Electron. Lett.*, vol. 55, no. 7, pp. 417–420, Apr. 2019.

[31] V. S. Asadchy, A. Wickberg, A. Díaz-Rubio, and M. Wegener, "Eliminating scattering loss in anomalously reflecting optical metasurfaces," *ACS Photon.*, vol. 4, no. 5, pp. 1264–1270, Apr. 2017.

[32] Y. Radi and A. Alü, "Reconfigurable metagratings," *ACS Photon.*, vol. 5, no. 5, 2018, Art. no. 17791785.

[33] A. Epstein and O. Rabinovich, "Analytical design of printed circuit board (PCB) metagratings for perfect anomalous reflection," *IEEE Trans. Antennas Propagation* vol. 66, no. 8, pp. 4086–4095, Aug. 2018.

[34] O. Rabinovich and A. Epstein, "Dual-polarized all-metallic metagratings for perfect anomalous reflection," *Phys. Rev. A, Gen. Phys. Appl.*, vol. 14, no. 6, Dec. 2020, Art. no. 131105.

[35] N. L. Tsitsas and C. Valagiannopoulos, "Anomalous refraction into free space with all-dielectric binary metagratings," *Phys. Rev. Res.*, vol. 2, no. 3, Sep. 2020, Art. no. 033526.

[36] M. Z. Chen, W. Tang, J. Y. Dai, J. C. Ke, L. Zhang, C. Zhang, J. Yang, L. Li, Q. Cheng, S. Jin, and T. J. Cui, "Accurate and broadband manipulations of harmonic amplitudes and phases to reach 256 QAM millimeter-wave wireless communications by time-domain digital coding metasurface," *Nat. Sci. Rev.*, vol. 9, no. 1, Jan. 2022, Art. no. nwab134.

[37] J. Shabanpour, "Programmable anisotropic digital metasurface for independent manipulation of dual-polarized THz waves based on a voltage-controlled phase transition of VO2 microwires," *J. Mater. Chem. C*, vol. 8, no. 21, pp. 7189–7199, Jun. 2020.

[38] O. Yurduseven, S. D. Assimonis, and M. Matthaiou, "Intelligent reflecting surfaces with spatial modulation: An electromagnetic perspective," *IEEE Open J. Commun. Soc.*, vol. 1, pp. 1256–1266, 2020.

[39] S.-K. Chou, O. Yurduseven, H. Q. Ngo, and M. Matthaiou, "On the aperture efficiency of intelligent reflecting surfaces," *IEEE Wireless Commun. Lett.*, vol. 10, no. 3, pp. 599–603, Mar. 2021.

[40] X. Chen, J. Shi, Z. Yang, and L. Wu, "Low-complexity channel estimation for intelligent reflecting surface-enhanced massive MIMO," *IEEE Wireless Commun. Lett.*, vol. 10, no. 5, pp. 996–1000, May 2021.

[41] J. C. Liang, Q. Cheng, Y. Gao, C. Xiao, S. Gao, L. Zhang, S. Jin, and T. J. Cui, "An angle-insensitive 3-bit reconfigurable intelligent surface," *IEEE Trans. Antennas Propag.*, vol. 70, no. 10, pp. 8798–8808, Oct. 2022.

[42] W. Chen, L. Bai, W. Tang, S. Jin, W. X. Jiang, and T. J. Cui, "Angle-dependent phase shifter model for reconfigurable intelligent surfaces: Does the angle-reciprocity hold?" *IEEE Commun. Lett.*, vol. 24, no. 9, pp. 2060–2064, Sep. 2020.

[43] O. Luukkonen, F. Costa, C. R. Simovski, A. Monorchio, and S. A. Tretyakov, "A thin electromagnetic absorber for wide incidence angles and both polarizations," *IEEE Trans. Antennas Propag.*, vol. 57, no. 10, pp. 3119–3125, Oct. 2009.
[44] S. M. Hashemi, S. A. Tretyakov, M. Soleimani, and C. R. Simovski, "Dual-polarized angularly stable high-impedance surface," *IEEE Trans. Antennas Propag.*, vol. 61, no. 8, pp. 4101–4108, Aug. 2013.
[45] C. R. Simovski, P. de Maagt, and I. V. Melchakova, "High-impedance surfaces having stable resonance with respect to polarization and incidence angle," *IEEE Trans. Antennas Propag.*, vol. 53, no. 3, pp. 908–914, Mar. 2005.
[46] O. Luukkonen, "Simple and accurate analytical model of planar grids and high-impedance surfaces comprising metal strips or patches," *IEEE Trans. Antennas Propag.*, vol. 56, no. 6, pp. 1624–1632, Jun. 2008.
[47] C. R. Simovski, P. de Maagt, S. A. Tretyakov, M. Paquay, and A. A. Sochava, "Angular stabilisation of resonant frequency of artificial magnetic conductors for TE-incidence," *Electron. Lett.*, vol. 40, no. 2, pp. 92–93, Jan. 2004.
[48] S. A. Tretyakov and S. I. Maslovski, "Thin absorbing structure for all incidence angles based on the use of a high-impedance surface," *Microw. Opt. Technol. Lett.*, vol. 38, no. 3, pp. 175–178, Aug. 2003.
[49] O. Luukkonen, C. R. Simovski, and S. A. Tretyakov, "Grounded uniaxial material slabs as magnetic conductors," *Prog. Electromagn. Res. B*, vol. 15, pp. 267–283, 2009.
[50] S. Tretyakov, *Analytical Modeling in Applied Electromagnetics*. Boston, MA, USA: Artech House, 2003.
[51] D. Sievenpiper, L. Zhang, R. F. J. Broas, N. G. Alexopolous, and E. Yablonovitch, "High-impedance electromagnetic surfaces with a forbidden frequency band," *IEEE Trans. Microw. Theory Techn.*, vol. 47, no. 11, pp. 2059–2074, Nov. 1999.
[52] R. F. J. Broas, D. F. Sievenpiper, and E. Yablonovitch, "An application of high impedance ground planes to phased array antennas," *IEEE Trans. Antennas Propag.*, vol. 53, no. 4, pp. 1377–1381, Apr. 2005.
[53] R. Baggen, M. Martinez-Vazquez, J. Leiss, S. Holzwarth, L. S. Drioli, and P. de Maagt, "Low profile Galileo antenna using EBG technology," *IEEE Trans. Antennas Propag.*, vol. 56, no. 3, pp. 667–674, Mar. 2008.
[54] I. V. Mel'chakova and K. R. Simovskii, "Efficient simple analytic model of artificial impedance surfaces based on resonance microstrip grids," *J. Commun. Technol. Electron.*, vol. 53, no. 8, pp. 874–882, Aug. 2008.
[55] I. Anderson, "On the theory of self-resonant grids," *Bell Syst. Tech. J.*, vol. 54, no. 10, pp. 1725–1731, Dec. 1975.
[56] V. Tapio, I. Hemadeh, A. Mourad, A. Shojaeifard, and M. Juntti, "Survey on reconfigurable intelligent surfaces below 10 GHz," *EURASIP J. Wireless Commun. Netw.*, vol. 2021, no. 1, pp. 1–18, Dec. 2021.
[57] A. Abraray, D. Nunes, and S. Maslovski, "Analytical and numerical modeling of reconfigurable reflecting metasurfaces with capacitive memory," 2022, *arXiv:2203.11666*.
[58] M. Liu, R.-H. Jin, J.-P. Geng, and X. Liang, "Low-insertion loss pin diode switches using impedance-transformation networks," *Prog. Electromagn. Res. C*, vol. 34, pp. 195–202, 2013.
[59] K. M. Hock, "Error correction for diffraction and multiple scattering in free-space microwave measurement of materials," *IEEE Trans. Microw. Theory Techn.*, vol. 54, no. 2, pp. 648–659, Feb. 2006.

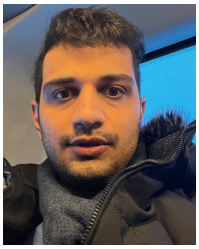

JAVAD SHABANPOUR (Graduate Student Member, IEEE) was born in Babol, Iran, in 1994. He received the B.Sc. degree in electrical engineering from the Babol Noshirvani University of Technology, Babol, Iran, in 2016, and the M.Sc. degree in communication-field and waves from the Iran University of Science and Technology (IUST), Tehran, Iran, in 2019. He is currently pursuing the Ph.D. degree with the Department of Electronics and Nanotechnology, Aalto University, Espoo, Finland. He is an Early Stage Researcher that worked on "Multi-function reconfigurable intelligent surfaces (RISs) structures for wireless networks." His current research interests include RIS, wireless communication, metamaterials, time-modulated metasurfaces, and applied electromagnetics.

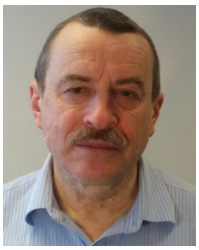

CONSTANTIN (KONSTANTIN) R. SIMOVSKI received the Ph.D. and H.D.R. degrees in physics and mathematics from St. Petersburg State Polytechnic University, Saint Petersburg, Russia, in 1986 and 2000, respectively. He was with both industry and academic institutions in several countries. From 2001 to 2008, he was a Full Professor at ITMO University, Saint Petersburg. Since 2008, he has been with Aalto University, Espoo, Finland, where he has been a Full professor, since 2012. He has authored and coauthored three scientific monographs and over 230 papers in refereed journals. His current research interests include metamaterials for optical sensing and energy harvesting, thermal radiation and radiative heat transfer on a nanoscale, antennas for magnetic resonance imaging, and wireless power transfer.